Resonant Modes in Shielded Uniaxial-Anisotropic Dielectric Rod Resonators

Yoshio Kobayashi, *Senior Member, IEEE,* and Tomohiro Senju

Abstract—**Rigorous field analyses by the mode matching method are presented for two types of dielectric rod resonators, including such uniaxial-anisotropic dielectrics as sapphire, which are placed between two parallel conducting plates (parallel-plates type) and in a conducting cavity (cavity-open type). For the parallel-plates-type resonator, the cutoff conditions of resonant modes are discussed. Resonant frequencies of some lowest order modes for these resonators are calculated, and mode charts are presented to design the resonators. The theory is verified by experiments.**

I. Introduction

RECENTLY, sapphire dielectric resonators placed between two parallel high-T_c superconducting films have attracted special interest since they realize a very high Q characteristic of over 2×10^6 below 90 K [1]. As is well known, single crystalline sapphires have relative permittivity perpendicular to the c-axis $\epsilon_t = 9.4$, and one parallel to the c-axis $\epsilon_z = 11.6$, because of their dielectric uniaxial anisotropy. Therefore, when designing such resonators, we need to take into account the influence of the anisotropic property on the resonant modes.

Analyses for uniaxial-anisotropic dielectric resonators have been performed rigorously by Krupka [2] using the Galerkin–Rayleigh–Ritz method, and approximately by Tobar *et al.* [3]. However, the calculated results presented by them are not sufficient for resonator designs. On the other hand, rigorous analyses for shielded isotropic dielectric rod resonators have been performed successfully by using the mode matching methods of two types; one is the radial mode matching method developed by Kobayashi *et al.* [4], [5], and the other is the axial mode matching method developed by Zaki *et al.* [6], [7]. The former method is useful to calculate the resonant modes systematically by a relatively simple procedure. On the other hand, for the latter method, we need a more complicated procedure because of the requirement of considering the guided complex modes.

In this paper, rigorous field analysis by the former method is discussed for shielded uniaxial-anisotropic dielectric rod resonators of two types; one is placed between two parallel conducting plates (parallel-plates type) and the other is centered in a conducting cavity (cavity-open type). Characteristic equations for these resonators are derived, resonant frequencies of some lowest order modes are calculated, and mode charts are presented to design these resonators. The validity of the theory is confirmed by experiments.

Manuscript received April 1, 1993; revised June 15, 1993.

The authors are with Department of Electrical and Electronic Engineering, Saitama University, Urawa, Saitama 338, Japan.

IEEE Log Number 9213003.

II. Analysis

A. Wave Equations

Fig. 1 shows two resonator structures to be analyzed in a cylindrical coordinate system r, θ, z; one is a parallel-plates-type resonator, where a dielectric rod is placed between two parallel, infinitely large conducting plates shown in Fig. 1(a); and the other is a cavity-open-type resonator, where the rod is placed symmetrically in a cylindrical conducting cavity shown in Fig. 1(b). The dielectric rod is assumed to have lossless homogeneous uniaxial-anisotropic characteristic with the c-axis of the dielectric parallel to the z-axis. Defining ϵ_t and ϵ_z as the relative permittivity perpendicular and parallel to the c-axis, respectively, the relative permittivity tensor $[\epsilon_r]$ is given by

$$[\epsilon_r] = \begin{bmatrix} \epsilon_t & 0 & 0 \\ 0 & \epsilon_t & 0 \\ 0 & 0 & \epsilon_z \end{bmatrix}. \tag{1}$$

The relative permeability of the dielectric is assumed to be $\mu_r = 1$, and the conductor is also assumed to be lossless.

Omitting a time-harmonic factor $e^{j\omega t}$, we can write Maxwell's equations for a source-free case in the medium $[\epsilon_r]$ as follows:

$$\nabla \times \boldsymbol{E} = -j\omega\mu_0 \boldsymbol{H} \tag{2}$$

$$\nabla \times \boldsymbol{H} = j\omega\epsilon_0 [\epsilon_r] \boldsymbol{E} \tag{3}$$

$$\nabla \cdot ([\epsilon_r]\boldsymbol{E}) = 0 \tag{4}$$

$$\nabla \cdot \boldsymbol{H} = 0 \tag{5}$$

where $\boldsymbol{E}$ and $\boldsymbol{H}$ are the electric and magnetic fields, ϵ_0 and μ_0 are the permittivity and permeability in vacuum, respectively. Then (4) can be rewritten as follows:

$$\nabla \cdot ([\epsilon_r]\boldsymbol{E}) = \epsilon_t \nabla \cdot \boldsymbol{E} - \epsilon_t \left(1 - \frac{\epsilon_z}{\epsilon_t}\right) \frac{\partial E_z}{\partial z} = 0. \tag{6}$$

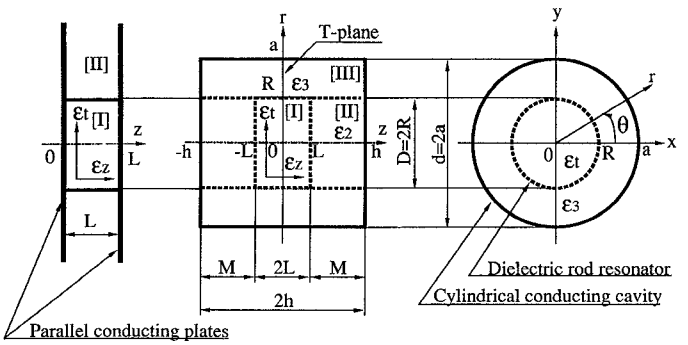

Fig. 1. Structures of shielded dielectric rod resonators. (a) Parallel-plates type. (b) Cavity-open type.

Thus, we obtain

$$\nabla \cdot \boldsymbol{E} = \left(1 - \frac{\epsilon_z}{\epsilon_t}\right) \frac{\partial E_z}{\partial z}. \tag{7}$$

In order to systematically analyze the resonant modes known to be hybrid in general, we derive two wave equations for z components of $\boldsymbol{E}$ and $\boldsymbol{H}$ below. At first, taking the rotation of (2) and using (3), we obtain

$$\nabla \times (\nabla \times \boldsymbol{E}) - k_0^2[\epsilon_r]\boldsymbol{E} = 0 \tag{8}$$

where $k_0^2 = \omega^2 \epsilon_0 \mu_0$. Using the vector formula

$$(\nabla \cdot \nabla)\boldsymbol{E} = \nabla(\nabla \cdot \boldsymbol{E}) - \nabla \times (\nabla \times \boldsymbol{E}) \tag{9}$$

and (7), equation (8) yields

$$(\nabla \cdot \nabla)\boldsymbol{E} - \left(1 - \frac{\epsilon_z}{\epsilon_t}\right) \nabla \left(\frac{\partial E_z}{\partial z}\right) + k_0^2[\epsilon_r]\boldsymbol{E} = 0. \tag{10}$$

The z component of (10) yields the following wave equation for E_z:

$$\nabla^2 E_z - \left(1 - \frac{\epsilon_z}{\epsilon_t}\right) \frac{\partial^2 E_z}{\partial z^2} + \epsilon_z k_0^2 E_z = 0 \tag{11}$$

where ∇^2 is the Laplacian.

Similarly, taking the rotation of (3) and using (5) and (9), we obtain

$$(\nabla \cdot \nabla)\boldsymbol{H} + j\omega\epsilon_0 \nabla \times ([\epsilon_r]\boldsymbol{E}) = 0. \tag{12}$$

Using (2), we rewrite the z component of the second term of the left-hand side of (12) as follows:

$$\{\nabla \times ([\epsilon_r]\boldsymbol{E})\}_z = \epsilon_t (\nabla \times \boldsymbol{E})_z = -j\omega\mu_0\epsilon_t H_z. \tag{13}$$

The combination of the z component of (12) and (13) yields the following wave equation for H_z:

$$\nabla^2 H_z + \epsilon_t k_0^2 H_z = 0. \tag{14}$$

B. Parallel-Plates-Type Resonators

We derive a characteristic equation for the parallel-plates-type resonator shown in Fig. 1(a) below. The quantities for homogeneous regions [I] and [II] are denoted by subscripts 1 and 2, respectively. In the region [II], $[\epsilon_r]$ is given by the unit matrix. The solutions of (11) and (14) are given by

$$E_{z1} = k_{e1}^2 A_e J_n(k_{e1} r) \cos n\theta \cos \beta z \tag{15}$$

$$H_{z1} = k_{m1}^2 A_m J_n(k_{m1} r) \sin n\theta \sin \beta z \tag{16}$$

in the region [I] ($0 \le r \le R$) and

$$E_{z2} = k_2^2 B_e K_n(k_2 r) \cos n\theta \cos \beta z \tag{17}$$

$$H_{z2} = k_2^2 B_m K_n(k_2 r) \sin n\theta \sin \beta z \tag{18}$$

in the region [II] ($r > R$), where

$$k_{e1}^2 = \epsilon_z k_0^2 - \frac{\epsilon_z}{\epsilon_t}\beta^2 \qquad k_{m1}^2 = \epsilon_t k_0^2 - \beta^2 \tag{19}$$

$$k_2^2 = \beta^2 - k_0^2 \tag{20}$$

$$\beta = \frac{2\pi}{\lambda_g} = \frac{l\pi}{L}; \qquad l = 0, 1, 2, \cdots \tag{21}$$

$$k_0 = \frac{2\pi}{\lambda_0} = \frac{2\pi f_0}{c} \tag{22}$$

and A_e, A_m, B_e, and B_m, which are multiplied by k_e^2 and k_m^2 for convenience of analysis described below, are constants determined from the boundary conditions. Also, n, m, and l denote the mode numbers in the azimuthal, radial, and axial directions, respectively. β is the axial wave number, λ_g is the axial wavelength, and λ_0 is the free-space wavelength. $J_n(x)$ and $K_n(x)$ are the Bessel function of the first kind and the modified Bessel function of the second kind, respectively. The field components except E_z and H_z are obtained by substituting (15)–(18) into the following relations [5]:

$$\begin{aligned}
E_r &= -j\omega\mu_0 \frac{1}{k_m^2}\frac{1}{r}\frac{\partial H_z}{\partial \theta} + \frac{\epsilon_z}{\epsilon_t}\frac{1}{k_e^2}\frac{\partial^2 E_z}{\partial r \partial z} \\
E_\theta &= j\omega\mu_0 \frac{1}{k_m^2}\frac{\partial H_z}{\partial r} + \frac{\epsilon_z}{\epsilon_t}\frac{1}{k_e^2}\frac{1}{r}\frac{\partial^2 E_z}{\partial \theta \partial z} \\
H_r &= \frac{1}{k_m^2}\frac{\partial^2 H_z}{\partial r \partial z} + j\omega\epsilon_0\epsilon_z \frac{1}{k_e^2}\frac{1}{r}\frac{\partial E_z}{\partial \theta} \\
H_\theta &= \frac{1}{k_m^2}\frac{1}{r}\frac{\partial^2 H_z}{\partial \theta \partial z} - j\omega\epsilon_0\epsilon_z \frac{1}{k_e^2}\frac{\partial E_z}{\partial r}
\end{aligned} \tag{23}$$

where k_m and k_e are the wave numbers in the radial direction.

The continuity of the tangential components of $\boldsymbol{E}$ and $\boldsymbol{H}$ between the regions [I] and [II] yields the following characteristic equation for the hybrid modes:

$$\left[\epsilon_z \frac{J_n'(u_e)}{u_e J_n(u_e)} + \frac{K_n'(v)}{v K_n(v)}\right]\left[\frac{J_n'(u_m)}{u_m J_n(u_m)} + \frac{K_n'(v)}{v K_n(v)}\right] = \frac{n^2\beta^2}{k_0^2}\left(\frac{1}{u_m^2} + \frac{1}{v^2}\right)^2 \tag{24}$$

where $u_e = k_{e1}R$, $u_m = k_{m1}R$, and $v = k_2 R$. The primes

on the Bessel functions refer to differentiation with respect to their argument x. Equation (24) is different from the one presented by Tobar *et al.* [3], in which the divergence of $\boldsymbol{E}$ is assumed not to depend on z with reference to (7).

When $n = 0$, particularly, (24) is divided into two groups; that is,

$$\frac{J_0'(u_m)}{u_m J_0(u_m)} + \frac{K_0'(v)}{vK_0(v)} = 0 \tag{25}$$

for the TE_{0ml} modes and

$$\epsilon_z \frac{J_0'(u_e)}{u_e J_0(u_e)} + \frac{K_0'(v)}{vK_0(v)} = 0 \tag{26}$$

for the TM_{0ml} modes. Also, when $l = 0$, (24) yields

$$\epsilon_z \frac{J_n'(u_e)}{u_e J_n(u_e)} + \frac{K_n'(v)}{vK_n(v)} = 0 \tag{27}$$

for the TM_{nm0} modes [4].

C. Cavity-Open-Type Resonators

The resonant modes for the structure shown in Fig. 1(b) are rigorously analyzed by the radial mode matching method similar to the isotropic case. From the symmetry of the structure, the resonant modes can be classified into those for which the T-plane (the r-θ plane at $z = 0$) is an electric wall and those for which it is a magnetic wall. In the following discussion, both types of modes are treated together. The equations are distinguished by using { } in which the upper and lower expressions correspond to the electric T-plane modes and the magnetic T-plane modes, respectively. From the symmetry of the structure, it is sufficient to consider only the region $z \geqq 0$, which is divided into three homogeneous regions [I], [II], and [III]. Applying the boundary conditions on the conducting surface and on the T-plane to the solutions of (11) and (14), we can expand H_z and E_z for each region as follows:

$$H_{z1} = \sin n\theta \sum_{p=1}^{\infty} A_{mp} k_{m1p}^2 J_n(k_{m1p} r) \begin{Bmatrix} \sin \beta_{m1p} z \\ \cos \beta_{m1p} z \end{Bmatrix} \tag{28}$$

$$H_{z2} = \sin n\theta \sum_{p=1}^{\infty} B_{mp} k_{m1p}^2 J_n(k_{m1p} r) \sin \beta_{m2p}(z - h) \tag{29}$$

$$H_{z3} = -\sin n\theta \sum_{q=1}^{\infty} C_{mq} k_{m3q}^2 F_n(k_{m3q} r) \begin{Bmatrix} \sin \beta_{m3q} z \\ \cos \beta_{m3q} z \end{Bmatrix} \tag{30}$$

$$E_{z1} = \cos n\theta \sum_{p=1}^{\infty} A_{ep} k_{e1p}^2 J_n(k_{e1p} r) \begin{Bmatrix} \cos \beta_{e1p} z \\ \sin \beta_{e1p} z \end{Bmatrix} \tag{31}$$

$$E_{z2} = \cos n\theta \sum_{p=1}^{\infty} B_{ep} k_{e1p}^2 J_n(k_{e1p} r) \cos \beta_{e2p}(z - h) \tag{32}$$

$$E_{z3} = -\cos n\theta \begin{Bmatrix} \sum_{q=0}^{\infty} C_{eq} k_{e3q}^2 G_n(k_{e3q} r) \cos \beta_{e3q} z \\ \sum_{q=1}^{\infty} C_{eq} k_{e3q}^2 G_n(k_{e3q} r) \sin \beta_{e3q} z \end{Bmatrix} \tag{33}$$

where

$$\left.\begin{aligned} F_n(x) &= I_n(x) - \frac{I_n'(k_{m3q}a)}{K_n'(k_{m3q}a)} K_n(x) \\ G_n(x) &= I_n(x) - \frac{I_n(k_{e3q}a)}{K_n(k_{e3q}a)} K_n(x) \end{aligned}\right\} \tag{34}$$

$$\left.\begin{aligned} k_{m1p}^2 &= \epsilon_t k_0^2 - \beta_{m1p}^2 = \epsilon_2 k_0^2 - \beta_{m2p}^2 \\ k_{m3q}^2 &= \beta_{m3q}^2 - \epsilon_3 k_0^2 \\ k_{e1p}^2 &= \epsilon_z k_0^2 - \frac{\epsilon_z}{\epsilon_t} \beta_{e1p}^2 = \epsilon_2 k_0^2 - \beta_{e2p}^2 \\ k_{e3q}^2 &= \beta_{e3q}^2 - \epsilon_3 k_0^2 \end{aligned}\right\} \tag{35}$$

$$\left.\begin{aligned} \beta_{m3q} &= \begin{Bmatrix} q\pi/h \\ (2q-1)\pi/2h \end{Bmatrix}; \quad q = 1, 2, 3, \cdots \\ \beta_{e3q} &= \begin{Bmatrix} q\pi/h; & q = 0, 1, 2, \cdots \\ (2q-1)\pi/2h; & q = 1, 2, 3, \cdots \end{Bmatrix} \end{aligned}\right\} . \tag{36}$$

In the above, $I_n(x)$ is the modified Bessel function of the first kind. A_{mp}, B_{mp}, C_{mq}, A_{ep}, B_{ep}, and C_{eq} are expansion coefficients to be determined from the boundary conditions for the regions [I], [II], and [III]. The other electromagnetic field components except H_z and E_z in each region are obtained by substituting (28)–(33) into (23).

From the continuity of E_θ and H_r at $z = L$, we first obtain

$$\frac{B_{mp}}{A_{mp}} = \begin{Bmatrix} -\dfrac{\sin X_{mp}}{\sin Y_{mp}} = \dfrac{M}{L} \dfrac{X_{mp} \cos X_{mp}}{Y_{mp} \cos Y_{mp}} \\ -\dfrac{\cos X_{mp}}{\sin Y_{mp}} = -\dfrac{M}{L} \dfrac{X_{mp} \sin X_{mp}}{Y_{mp} \cos Y_{mp}} \end{Bmatrix} \tag{37}$$

$$\frac{B_{ep}}{A_{ep}} = \begin{Bmatrix} \dfrac{\epsilon_z}{\epsilon_2} \dfrac{\cos X_{ep}}{\cos Y_{ep}} = -\dfrac{\epsilon_z}{\epsilon_t} \dfrac{M}{L} \dfrac{X_{ep} \sin X_{ep}}{Y_{ep} \sin Y_{ep}} \\ \dfrac{\epsilon_z}{\epsilon_2} \dfrac{\sin X_{ep}}{\cos Y_{ep}} = \dfrac{\epsilon_z}{\epsilon_t} \dfrac{M}{L} \dfrac{X_{ep} \cos X_{ep}}{Y_{ep} \sin Y_{ep}} \end{Bmatrix} \tag{38}$$

with $X_{mp} = \beta_{m1p} L$, $Y_{mp} = \beta_{m2p} M$, $X_{ep} = \beta_{e1p} L$, and $Y_{ep} = \beta_{e2p} M$. Furthermore, (X_{mp}, Y_{mp}) is given as the pth root of the following simultaneous equations:

$$\left.\begin{aligned} \begin{Bmatrix} -X_{mp} \cot X_{mp} \\ X_{mp} \tan X_{mp} \end{Bmatrix} &= \frac{L}{M} Y_{mp} \cot Y_{mp} \\ \left(\frac{X_{mp}}{L}\right)^2 - \left(\frac{Y_{mp}}{M}\right)^2 &= k_0^2(\epsilon_t - \epsilon_2) \end{aligned}\right\} \tag{39}$$

while (X_{ep}, Y_{ep}) is the pth root of the following:

$$\left.\begin{aligned} \begin{Bmatrix} -X_{ep} \tan X_{ep} \\ X_{ep} \cot X_{ep} \end{Bmatrix} &= \frac{\epsilon_t}{\epsilon_2} \frac{L}{M} Y_{ep} \tan Y_{ep} \\ \frac{\epsilon_z}{\epsilon_t} \left(\frac{X_{ep}}{L}\right)^2 - \left(\frac{Y_{ep}}{M}\right)^2 &= k_0^2(\epsilon_z - \epsilon_2) \end{aligned}\right\} \tag{40}$$

where the integer p is counted in increasing order. These equations were derived from (35), (37), and (38).

From the continuity of H_z at $r = R$, we then obtain

$$\left.\begin{aligned}&\sum_{p=1}^{\infty} A_{mp}u_{mp}^2 J_n(u_{mp})\begin{Bmatrix}\sin(X_{mp}z/L)\\ \cos(X_{mp}z/L)\end{Bmatrix}; \quad 0 \le z \le L\\ &\sum_{p=1}^{\infty} B_{mp}u_{mp}^2 J_n(u_{mp})\sin(Y_{mp}(z-h)/M);\\ &\quad L < z \le h\end{aligned}\right\}$$
$$= -\sum_{q=1}^{\infty} C_{mq}v_{mq}^2 F_n(v_{mq})\begin{Bmatrix}\sin\beta_{m3q}z\\ \cos\beta_{m3q}z\end{Bmatrix}; \quad 0 \le z \le h \tag{41}$$

with $u_{mp} = k_{m1p}R$ and $v_{mq} = k_{m3q}R$. Multiplying

$$\begin{Bmatrix}\sin\beta_{m3q}z\\ \cos\beta_{m3q}z\end{Bmatrix}; \quad q = 1, 2, 3, \cdots$$

on both sides of (41) and integrating from 0 to h with respect to z, we obtain the following expression from the orthogonality of trigonometric functions:

$$\sum_{p=1}^{\infty} A_{mp}u_{mp}^2 J_n(u_{mp})\left[P_{pq}^m + \frac{B_{mp}}{A_{mp}}Q_{pq}^m\right] = -C_{mq}v_{mq}^2 F_n(v_{mq})h/2. \tag{42}$$

Similarly, the continuity of E_z yields

$$\sum_{p=1}^{\infty} A_{ep}u_{ep}^2 J_n(u_{ep})\left[R_{pq}^e + \frac{B_{ep}}{A_{ep}}S_{pq}^e\right] = -C_{eq}v_{eq}^2 G_n(v_{eq}) \cdot \begin{Bmatrix}\epsilon_q h/2; & q = 0, 1, 2, \cdots\\ h/2; & q = 1, 2, 3, \cdots\end{Bmatrix} \tag{43}$$

with $u_{ep} = k_{e1p}R$, $v_{ep} = k_{e3q}R$, and

$$\epsilon_q = \begin{cases}2; & q = 0\\ 1; & q \ge 1\end{cases}$$

where

$$\begin{aligned}P_{pq}^m &= \int_0^L \begin{Bmatrix}\sin(X_{mp}z/L)\sin\beta_{m3q}z\\ \cos(X_{mp}z/L)\cos\beta_{m3q}z\end{Bmatrix} dz\\ Q_{pq}^m &= \int_L^h \sin\frac{Y_{mp}}{M}(z-h)\begin{Bmatrix}\sin\beta_{m3q}z\\ \cos\beta_{m3q}z\end{Bmatrix} dz\\ R_{pq}^e &= \int_0^L \begin{Bmatrix}\cos(X_{ep}z/L)\cos\beta_{e3q}z\\ \sin(X_{ep}z/L)\sin\beta_{e3q}z\end{Bmatrix} dz\\ S_{pq}^e &= \int_L^h \cos\frac{Y_{ep}}{M}(z-h)\begin{Bmatrix}\cos\beta_{e3q}z\\ \sin\beta_{e3q}z\end{Bmatrix} dz.\end{aligned} \tag{44}$$

Substituting (42) and (43) into the continuity conditions of E_θ and H_θ to eliminate C_{eq} and C_{mq}, we obtain the following homogeneous equations for the expansion coefficients $\tilde{A}_{mp} = jA_{mp}u_{mp}^2 J_n(u_{mp})$ and $\tilde{A}_{ep} = A_{ep}u_{ep}^2 J_n(u_{ep})$[5]:

$$\begin{aligned}&\omega\mu_0 \sum_{p=1}^{\infty}\tilde{A}_{mp}\left[\frac{F_n'(v_{mq})}{v_{mq}F_n(v_{mq})} + \frac{J_n'(u_{mp})}{u_{mp}J_n(u_{mp})}\right]\cdot\left[P_{pq}^m + \frac{B_{mp}}{A_{mp}}Q_{pq}^m\right]\\ &\pm n\sum_{p=1}^{\infty}\tilde{A}_{ep}\left[\frac{1}{u_{ep}^2}\left(\frac{\epsilon_z}{\epsilon_t}\frac{X_{ep}}{L}P_{pq}^e \pm \frac{B_{ep}}{A_{ep}}\frac{Y_{ep}}{M}Q_{pq}^e\right) + \frac{\beta_{e3q}}{v_{eq}^2}\left(R_{pq}^e + \frac{B_{ep}}{A_{ep}}S_{pq}^e\right)\right] = 0\\ &\qquad q = 1, 2, 3, \cdots\end{aligned} \tag{45}$$

$$\begin{aligned}&n\sum_{p=1}^{\infty}\tilde{A}_{mp}\left[\frac{1}{u_{mp}^2}\left(\frac{X_{mp}}{L}R_{pq}^m \pm \frac{B_{mp}}{A_{mp}}\frac{Y_{mp}}{M}S_{pq}^m\right) + \frac{\beta_{m3q}}{v_{mq}^2}\left(P_{pq}^m + \frac{B_{mp}}{A_{mp}}Q_{pq}^m\right)\right]\\ &\pm \omega\epsilon_0\sum_{p=1}^{\infty}\tilde{A}_{ep}\left[\frac{\epsilon_3 G_n'(v_{eq})}{v_{eq}G_n(v_{eq})}\left(R_{pq}^e + \frac{B_{ep}}{A_{ep}}S_{pq}^e\right) + \frac{J_n'(u_{ep})}{u_{ep}J_n(u_{ep})}\left(\epsilon_z R_{pq}^e + \epsilon_2\frac{B_{ep}}{A_{ep}}S_{pq}^e\right)\right] = 0\\ &\qquad q = \begin{Bmatrix}0, 1, 2, \cdots\\ 1, 2, 3, \cdots\end{Bmatrix}.\end{aligned} \tag{46}$$

In (45) and (46), the upper and lower signs correspond to the electric T-plane modes and the magnetic T-plane modes, respectively. Furthermore, P_{pq}^m, Q_{pq}^m, R_{pq}^e, and S_{pq}^e are given by (44), while P_{pq}^e, Q_{pq}^e, R_{pq}^m, and S_{pq}^m can be obtained by interchanging e and m in (44).

For $\tilde{A}_{mp}$ and $\tilde{A}_{ep}$, which are not zero simultaneously in (45) and (46), the determinant of the coefficient matrix needs to be zero. Accordingly, this requirement yields the following $N \times N$ square determinant as a characteristic equation for the hybrid modes:

$$\det[H_{ij}] = 0; \quad i, j = 1, 2, 3, \cdots, N \tag{47}$$

where the matrix elements H_{ij} are given by

$$\begin{aligned}H_{2q\pm1,2p-1} &= \omega\epsilon_0\left[\frac{\epsilon_3 G_n'(v_{eq})}{v_{eq}G_n(v_{eq})}\left(R_{pq}^e + \frac{B_{ep}}{A_{ep}}S_{pq}^e\right) + \frac{J_n'(u_{ep})}{u_{ep}J_n(u_{ep})}\left(\epsilon_z R_{pq}^e + \epsilon_2\frac{B_{ep}}{A_{ep}}S_{pq}^e\right)\right]\\ H_{2q\pm1,2p} &= n\left[\frac{1}{u_{mp}^2}\left(\frac{X_{mp}}{L}R_{pq}^m \pm \frac{B_{mp}}{A_{mp}}\frac{Y_{mp}}{M}S_{pq}^m\right) + \frac{\beta_{m3q}}{v_{mq}^2}\left(P_{pq}^m + \frac{B_{mp}}{A_{mp}}Q_{pq}^m\right)\right]\\ &\qquad p = 1, 2, 3, \cdots\\ &\qquad q = \begin{Bmatrix}0, 1, 2, \cdots\\ 1, 2, 3, \cdots\end{Bmatrix}\end{aligned} \tag{48}$$

$$H_{2q,2p-1} = n\left[\frac{1}{u_{ep}^2}\left(\frac{\epsilon_z}{\epsilon_t}\frac{X_{ep}}{L}P_{pq}^e \pm \frac{B_{ep}}{A_{ep}}\frac{Y_{ep}}{M}Q_{pq}^e\right) + \frac{\beta_{e3q}}{v_{eq}^2}\left(R_{pq}^e + \frac{B_{ep}}{A_{ep}}S_{pq}^e\right)\right]$$

$$H_{2q,2p} = \omega\mu_0\left[\frac{F_n'(v_{mq})}{v_{mq}F_n(v_{mq})} + \frac{J_n'(u_{mp})}{u_{mp}J_n(u_{mp})}\right] \cdot \left[P_{pq}^m + \frac{B_{mp}}{A_{mp}}Q_{pq}^m\right]$$

$$p, q = 1, 2, 3, \cdots. \tag{49}$$

As the size of the matrix N is increased, the solutions approach true values. In actual calculations, N is chosen so that the solution may converge to within desired accuracy. For the magnetic T-plane modes, we take $N = 2q$ because the TM_{nm0} modes do not exist in this case. On the other hand, for the electric T-plane modes, we take $N = 2q + 1$ consisting of $q + 1$ terms from (48), where the TM_{nm0} modes corresponding to $q = 0$ do exist, and q terms from (49).

When $n = 0$ in (45) and (46), particularly, the matrix elements are given by

$$H_{qp} = \left[\frac{F_0'(v_{mq})}{v_{mq}F_0(v_{mq})} + \frac{J_0'(u_{mp})}{u_{mp}J_0(u_{mp})}\right] \cdot \left[P_{pq}^m + \frac{B_{mp}}{A_{mp}}Q_{pq}^m\right]$$

$$p, q = 1, 2, 3, \cdots \tag{50}$$

for the TE_0 modes and

$$H_{\{q}^{q+1\}p} = \left[\frac{\epsilon_3 G_0'(v_{eq})}{v_{eq}G_0(v_{eq})}\left(R_{pq}^e + \frac{B_{ep}}{A_{ep}}S_{pq}^e\right) + \frac{J_0'(u_{ep})}{u_{ep}J_0(u_{ep})}\left(\epsilon_z R_{pq}^e + \epsilon_2\frac{B_{ep}}{A_{ep}}S_{pq}^e\right)\right]$$

$$p = 1, 2, 3, \cdots$$

$$q = \begin{cases} 0, 1, 2, \cdots \\ 1, 2, 3, \cdots \end{cases} \tag{51}$$

for the TM_0 modes.

III. Calculations

A. Parallel-Plates-Type Resonators

For the parallel-plates-type resonator, (24)–(27) were calculated in a similar way to the isotropic case [4]. The results for some lowest order modes are shown in Fig. 2 as a mode chart, in which solid curves indicate the case of $\epsilon_t = \epsilon_z = 10$, and broken curves denote the case of $\epsilon_t = 10$ and $\epsilon_z = 12$. The TE_{011} mode is independent of ϵ_z because it has no E_z component. The broken curves for the HE_{111}, TE_{011}, TM_{011}, and HE_{211} modes show very good agreement with ones calculated by Krupka [2] using the Galerkin–Rayleigh–Ritz method. The anisotropic property affects the resonant frequencies more strongly in the order of the EH_{111}, HE_{111}, HE_{211}, and TM_{011} modes according to the strength of the E_z component.

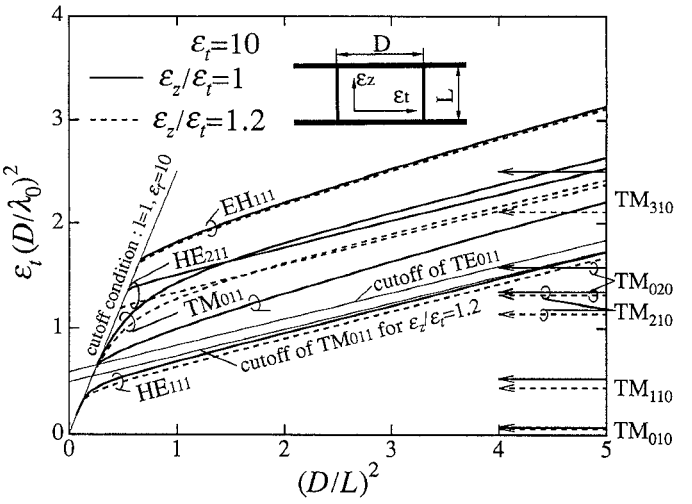

Fig. 2. Mode chart for the parallel-plates-type resonator.

The calculated curves described above indicate the resonances in a trapped state where the energy is confined in and near the rod without radiation [4]. These trapped states are cut off at particular values of $(D/L)^2$, namely, $(D/L)_c^2$. The cutoff conditions for the anisotropic case were derived in a similar way to the procedure performed by Snitzer [8]. The complete derivations are given elsewhere [9]. In particular, the cutoff condition for the TE_{0ml} and TM_{0ml} modes is given by

$$J_0(u_c) = 0 \tag{52}$$

where $u_c = k_c R$. Since $k_{m1} = k_{e1} = k_c$ and $k_0 = 2\pi/\lambda_c$ at the cutoff, where λ_c is the cutoff wavelength, the combination of (19) and (21) yields

$$\epsilon_t\left(\frac{D}{\lambda_c}\right)^2 = \frac{l^2}{4}\left(\frac{D}{L}\right)_c^2 + \left(\frac{u_c}{\pi}\right)^2 \tag{53}$$

for the TE_{0ml} modes and

$$\epsilon_t\left(\frac{D}{\lambda_c}\right)^2 = \frac{l^2}{4}\left(\frac{D}{L}\right)_c^2 + \frac{\epsilon_t}{\epsilon_z}\left(\frac{u_c}{\pi}\right)^2 \tag{54}$$

for the TM_{0ml} modes. These results are indicated by thin straight lines with the slope of $l^2/4$ in the figure. On the other hand, since (20) is expressed by $l\pi/L = 2\pi/\lambda_c$ at the cutoff, we obtain the following relation:

$$\epsilon_t\left(\frac{D}{\lambda_c}\right)^2 = \epsilon_t\frac{l^2}{4}\left(\frac{D}{L}\right)_c^2. \tag{55}$$

On the mode chart, (55) is indicated by a straight line which intersects the origin and has the slope of $\epsilon_t l^2/4$. In the isotropic case, the cutoff frequencies $f_c = c/\lambda_c$ for the TE_{0ml} and TM_{0ml} modes are the same, while in the anisotropic case, those for the TM_{0ml} modes are different

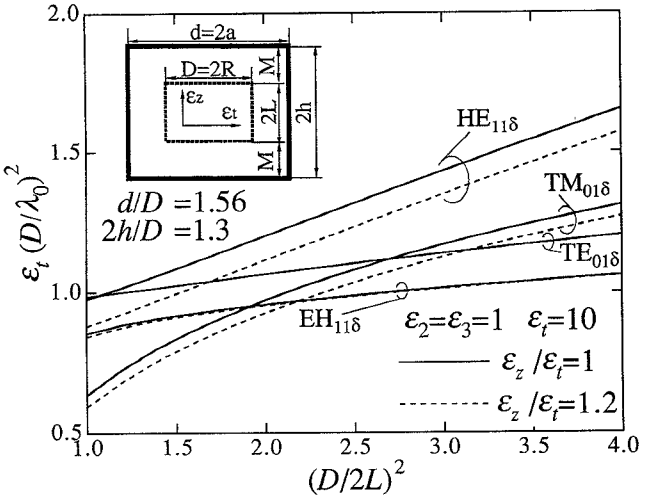

Fig. 3. Mode chart for the cavity-open-type resonator when $d/D = 1.56$ and $2h/D = 1.3$.

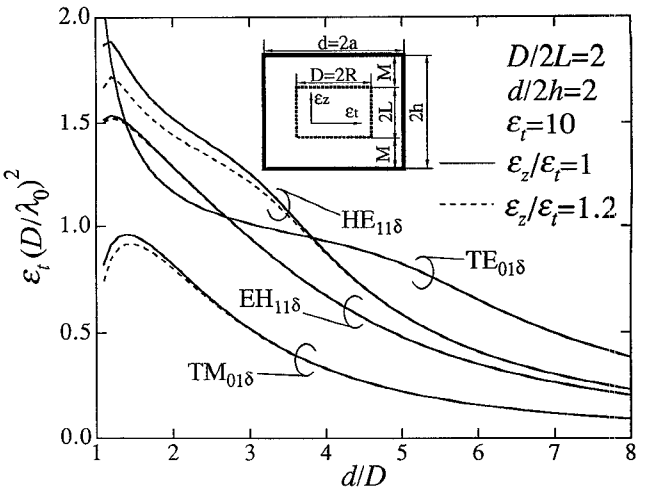

Fig. 4. Mode chart for the cavity-open-type resonator when $D/2L = 2$ and $d/2h = 2$.

from those for the TE_{0ml} modes. The left side region of the cutoff condition in the figure is in a leaky state, where part of the energy leaks away in the radial direction and radiation loss occurs. The TM_{nm0} modes are always in the leaky state and are independent of ϵ_t because they have only the E_z component; thus, we can directly use the calculated values presented in [4].

TABLE I
MEASURED VALUES OF ϵ_t AND ϵ_z FOR SAPPHIRES

Sample	D (mm)	L (mm)	f_0 (GHz)		ϵ_t	ϵ_z
			TE_{011}	TM_{011}		
1	9.985	9.998	9.741	10.949	9.389	11.478
2	10.002	5.002	13.551	14.261	9.399	11.553

B. Cavity-Open-Type Resonators

The resonant frequencies of some lowest order modes for the cavity-open-type resonator were calculated from (47)–(51). We took $N = 10$ for the $TE_{01\delta}$ mode, $N = 19$ for the $HE_{11\delta}$ mode, $N = 20$ for the $TM_{01\delta}$ mode, and $N = 30$ for the $EH_{11\delta}$ mode, so that the resonant frequencies may converge to within 0.01 percent. The results are shown in Fig. 3 as a mode chart. The case of $\epsilon_t = \epsilon_z = 10$ is indicated by solid curves, and the case of $\epsilon_t = 10$ and $\epsilon_z = 12$ by broken curves. It is found that the anisotropic property of materials strongly influences the resonant frequencies for the $TM_{01\delta}$ and $HE_{11\delta}$ modes, having the predominant E_z component, and weakly influences the ones for the $TE_{01\delta}$ and $EH_{11\delta}$ modes, having the predominant H_z component. For sapphire resonators having relatively low permittivity (about 10), the $TM_{01\delta}$ or $EH_{11\delta}$ mode becomes dominant according as the aspect ratio $(D/2L)^2$ is smaller or greater than 2. This is in contrast with the case of commonly used dielectric resonators with $\epsilon_t = \epsilon_z$ over 20, where the $TE_{01\delta}$ mode is dominant [10].

Another mode chart was calculated to investigate the dependence of the size of the conducting cavity on the resonant frequencies. The results are shown in Fig. 4. When $d/D < 4$, the uniaxial anisotropy considerably affects the frequencies. This means that most of the energy is stored in and near the dielectric rod. On the contrary, when $d/D > 4$, the resonant frequencies are not affected by the anisotropy, because most of the energy is stored outside the dielectric rod.

IV. EXPERIMENTS

In a way similar to that used by Krupka [2], we measured ϵ_t and ϵ_z for two samples of sapphire (KYOCERA Co. Ltd.) by constructing a parallel-plates-type resonator, where the diameter of two copper plates used is 50 mm. The ϵ_t values were determined from the f_0 values measured for the TE_{011} mode by solving (25). Then the ϵ_z values were determined from the f_0 values measured for the TM_{011} mode and the ϵ_t values measured above by using (26). The measured results are summarized in Table I. The mode chart was useful to identify the resonant modes for different resonant frequencies.

We performed experiments for cavity-open-type resonators to verify the calculations. Each of the sapphires described above is placed in the center of a copper cavity having $d = 15.55$ mm and $2h = 13.00$ mm, supported by foamed plastic having $\epsilon_2 = 1.031$. The frequency responses of the transmission-type resonators were measured using an HP network analyzer. Two semirigid cables with small loops were used to excite and detect both the H_z and H_θ components of the fields. The results are shown in Fig. 5. The calculated f_0 values are indicated on the top of the figures. The calculated and measured values of f_0 and the differences Δf_0 are summarized in Table II. It is found from Table II that the calculated f_0 values for three modes except the $TE_{01\delta}$ mode are a little higher than the measured values. This result is due to an inaccuracy of the measured ϵ_z values; the measured resonant frequencies of the TM_{0m1} modes for the parallel-plates-type re-

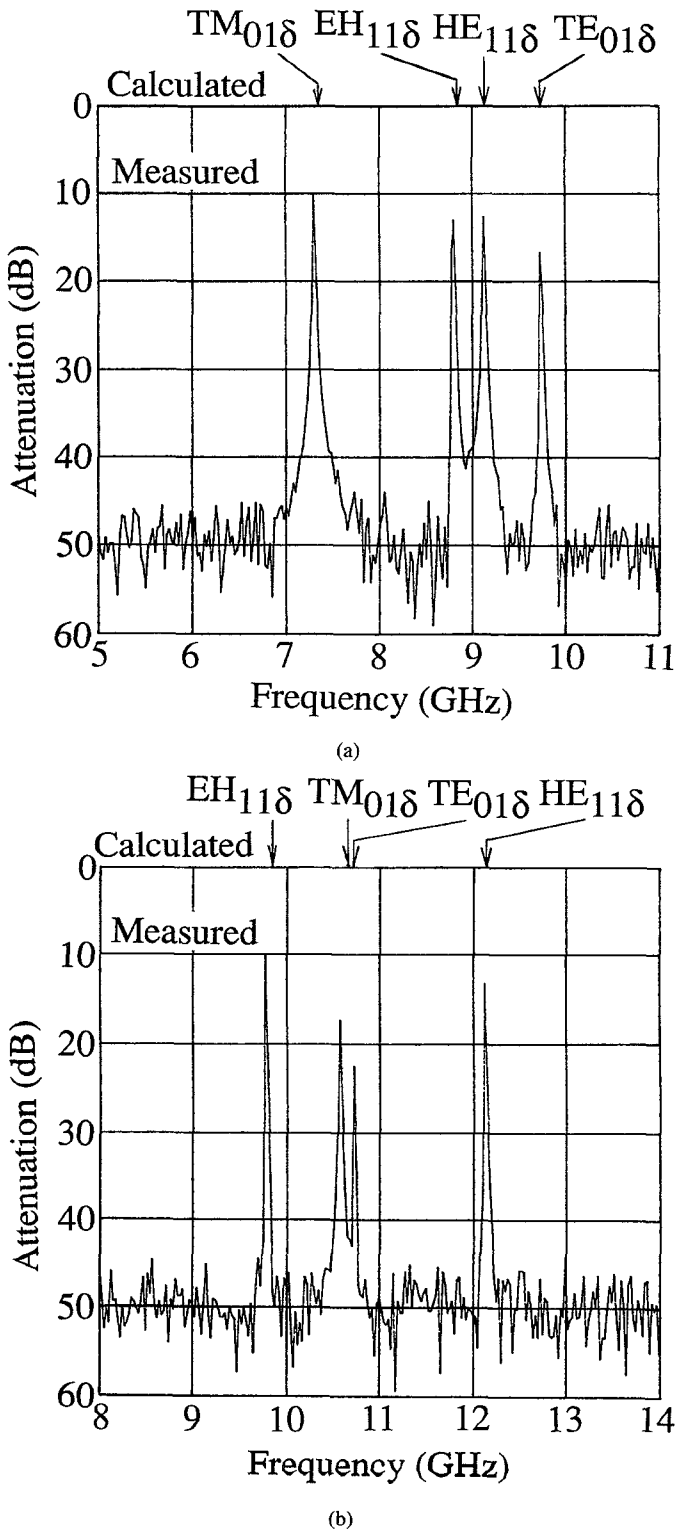

Fig. 5. Measured results and four identified resonant modes of the lowest order for the cavity-open-type resonator. (d = 15.55 mm, $2h$ = 13.00 mm, ϵ_2 = 1.031, ϵ_3 = 1.) (a) D = 9.985 mm, $2L$ = 9.998 mm, ϵ_t = 9.389, ϵ_z = 11.478. (b) D = 10.002 mm, $2L$ = 5.002 mm, ϵ_t = 9.399, ϵ_z = 11.553.

sonator have been increased due to the air gaps effect at the rod–plates interface, and then the ϵ_z values have been estimated lower than true ones.

TABLE II
COMPARISON OF CALCULATED RESONANT FREQUENCIES WITH MEASUREMENTS FOR TWO CAVITY-OPEN-TYPE SAPPHIRE RESONATORS WHEN d = 15.55 mm, $2h$ = 13.00 mm, ϵ_2 = 1.031, AND ϵ_3 = 1

(a) Sample 1 (D = 9.985 mm, 2L = 9.998 mm, ϵ_t = 9.389, ϵ_z = 11.478)

Resonant mode	$TM_{01\delta}$	$EH_{11\delta}$	$HE_{11\delta}$	$TE_{01\delta}$
f_0 (GHz) calculated	7.339	8.827	9.121	9.720
f_0 (GHz) measured	7.275	8.797	9.099	9.714
$\Delta f_0/f_0$ (%)	+0.88	+0.34	+0.24	+0.06

(b) Sample 2 (D = 10.002 mm, 2L = 5.002 mm, ϵ_t = 9.399, ϵ_z = 11.553)

Resonant mode	$EH_{11\delta}$	$TM_{01\delta}$	$TE_{01\delta}$	$HE_{11\delta}$
f_0 (GHz) calculated	9.841	10.664	10.704	12.153
f_0 (GHz) measured	9.795	10.577	10.706	12.138
$\Delta f_0/f_0$ (%)	+0.47	+0.82	-0.02	+0.12

V. CONCLUSIONS

It was verified that the mode matching method, commonly used for the analysis of isotropic dielectric resonators, can be applied successfully to the analysis of uniaxial-anisotropic dielectric resonators. The characteristic equations were derived for resonator structures of two types; the parallel-plates and cavity-open types. The cutoff conditions of the resonant modes for the parallel-plates-type resonator were discussed. The mode charts calculated from the characteristic equations are useful to design sapphire rod resonators of these two types.

REFERENCES

[1] Z. Y. Shen, C. Wilker, P. Pang, and W. Holstein, "High T_c superconductor-sapphire microwave resonator with extremely high Q-values up to 90 K," in *1992 IEEE MTT-S Int. Microwave Symp. Dig.*, F-3, pp. 193–196.

[2] J. Krupka, "Resonant modes in shielded cylindrical ferrite and single-crystal dielectric resonators," *IEEE Trans. Microwave Theory Tech.*, vol. MTT-37, pp. 691–697, Apr. 1989.

[3] M. E. Tobar and A. G. Mann, "Resonant frequencies of higher order modes in cylindrical anisotropic dielectric resonators," *IEEE Trans. Microwave Theory Tech.*, vol. MTT-39, pp. 2077–2082, Dec. 1991.

[4] Y. Kobayashi and S. Tanaka, "Resonant mode of a dielectric rod resonator short-circuited at both ends by parallel conducting plates," *IEEE Trans. Microwave Theory Tech.*, vol. MTT-28, pp. 1077–1085, Oct. 1980.

[5] Y. Kobayashi, N. Fukuoka, and S. Yoshida, "Resonant modes for a shielded dielectric rod resonator," *Electron. Commun. Japan*, vol. 64-B, no. 11, pp. 44–51, 1981.

[6] K. A. Zaki and A. E. Atia, "Modes in dielectric-loaded waveguides and resonators," *IEEE Trans. Microwave Theory Tech.*, vol. MTT-31, pp. 815–824, July 1986.

[7] C. Chen and K. A. Zaki, "Resonant frequencies of dielectric resonators containing guided complex modes," *IEEE Trans. Microwave Theory Tech.*, vol. MTT-36, pp. 1455–1457, Oct. 1988.

[8] E. Snitzer, "Cylindrical dielectric waveguide modes," *J. Opt. Soc. Amer.*, vol. 51, pp. 491–498, May 1961.

[9] Y. Kobayashi and T. Senju, "Anisotropic complex permittivity measurement of uniaxial dielectric rods by dielectric resonator method," 1993 Asia-Pacific Microwave Conf., Paper MET-081R-07.
[10] Y. Kobayashi and S. Nakayama, "Design charts for shielded dielectric rod and ring resonators," in *1986 IEEE MTT-S Int. Microwave Symp. Dig.*, J-8, pp. 241–244.

Yoshio Kobayashi (M'74–SM'91) was born on July 4, 1939. He received the B.E., M.E., and D.Eng. degrees in electrical engineering from Tokyo Metropolitan University, Tokyo, Japan, in 1963, 1965, and 1982, respectively.

He was a Research Assistant from 1965 to 1968, a Lecturer from 1968 to 1982, and an Associate Professor from 1982 to 1988 in the Department of Electrical Engineering, Saitama University, Urawa, Saitama, Japan. He is now a Professor at the same university. His current research interests are in dielectric resonators, dielectric filters, measurement of dielectric materials, and properties of high-Tc superconductors in the microwave and millimeter-wave region.

Dr. Kobayashi is a member of the IEICE of Japan and the IEE of Japan.

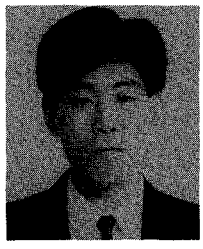

Tomohiro Senju was born in Saitama, Japan, on October 31, 1969. He received the B.E. degree in electrical engineering from Saitama University, Saitama, Japan, in 1993.

He is currently with the Department of Electrical and Electronic Engineering, Saitama University, working toward the M.E. degree. His research interests include dielectric resonators and microwave measurements of dielectric materials.

Mr. Senju is an associate member of the Institute of Electronics, Information, and Communication Engineering of Japan.